Available online at www.sciencedirect.com
SCIENCE DIRECT®
Catalysis Today 101 (2005) 307–314
CATALYSIS TODAY
www.elsevier.com/locate/cattod

Role of the support on the activity of silica-supported TiO_2 photocatalysts: Structure of the TiO_2/SBA-15 photocatalysts

María-José López-Muñoz *, Rafael van Grieken, José Aguado, Javier Marugán

ESCET, Universidad Rey Juan Carlos, C/Tulipán s/n, 28933 Móstoles, Madrid, Spain

Available online 25 March 2005

Abstract

Immobilization of TiO_2 on silica materials has been commonly proposed in order to make easier the separation of the catalyst after the photocatalytic reactions in aqueous systems. The main drawback of the supported photocatalysts is that they usually show lower activities in comparison with powdered TiO_2 materials. The aim of this work is to elucidate the structure of some silica-supported TiO_2 photocatalysts recently developed as well as to evaluate the role that the porous structure of the support can play in the observed photocatalytic activities. In comparison with the use of an amorphous silica support, the use of the mesostructured silica SBA-15 produces an ordered structure in which TiO_2 crystals of similar sizes, independently of titania loading, are located inside the mesoporous channels of the support. The photocatalytic treatment of several cyanide-containing compounds is analyzed and the results are explained in terms of the structure of every catalyst. Depending on the model compound, the characteristic structure of the TiO_2/SBA-15 materials allows increasing up to eight times the activity achieved by the Degussa P25 TiO_2. The main conclusion of this work is the strong influence of the textural properties of the support on the catalytic activity of immobilized TiO_2 photocatalysts.

Keywords: Photocatalysis; Silica-supported TiO_2; Cyanides

1. Introduction

Heterogeneous photocatalysis has shown a high efficiency in the removal of highly toxic and non-biodegradable pollutants commonly present in air and domestic or industrial wastewaters [1–7]. These processes are based on the use of UV radiation to stimulate a semiconductor material, usually TiO_2, on whose surface the oxidation of the pollutant is carried out.

To maximize TiO_2 photoactivity, particles should be small enough to offer a high specific surface area. Unfortunately, for applications in aqueous phase such a small particle size means high filtration costs to remove the catalyst once the reaction is finished. These problems have motivated the development of supported photocatalysts in which TiO_2 has been immobilized on diverse materials [8,9].

In addition to some other important properties, it is desirable for a support to be chemically inert, to present a high specific surface area and to be transparent to the UV radiation. Probably this is the reason why most of the work on immobilized photocatalysts has been focused to the use of siliceous materials as supports, for instance: non-porous silica microspheres [10,11], glass [12–15], quartz [13,16] and silica gel [17–25]. A special mention requires the use of silicates or aluminosilicates with zeolitic structures, either crystalline, such as VPI-5 [26] and zeolites X and Y [22,27,28], or mesostructured, such as FSM-16 [29], HMS [22] and MCM-41 [27–29].

Concerning the photocatalysts preparation methods, there are also many procedures reported in the literature. As examples: (i) flame oxidation of $TiCl_4$ [10], (ii) hydrolysis of $TiCl_3$ [11], (iii) chemical vapour deposition [12,24,25], (iv) oxidation of metallic titanium [16], (v) metal ion implantation [15], (vii) immobilization of commercial TiO_2 materials, e.g. Degussa P25 [21] and (vii) sol–gel [13,14,17–23].

Probably the most widely used materials consist of titanium dioxide synthesized via sol–gel and supported on silica gel. This combination allows a precise control of the properties of the produced materials through the manipulation of the main synthesis variables, in order to maximize

* Corresponding author. Tel.: +34 91 664 74 64; fax: +34 91 488 70 68
E-mail address: m.j.lopez@escet.urjc.es (M.-J. López-Muñoz).

0920-5861/$ – see front matter © 2005 Elsevier B.V. All rights reserved.
doi:10.1016/j.cattod.2005.03.017

the activity of the supported photocatalysts. However, and despite huge efforts, immobilized TiO_2 is commonly reported as less photoactive than the bare TiO_2, with only several exceptions in which the adsorption stage seems to control the global kinetics [30,31].

In a previous work, we reported the synthesis of a new type of supported photocatalysts obtained by controlling the crystal size of TiO_2 through the use of the mesostructured silica SBA-15 as support [32]. These materials presented a lower activity for free cyanide photoxidation than the commercial TiO_2 Degussa P25. However, they showed unexpected activities for cyanide photoxidation when iron-complexed species were present, leading to much better results than those corresponding to P25 [33]. The aim of the present work is to carry out a detailed characterization of these materials in order to clarify the influence of the structure of the silica support on the photocatalytic activity for several cyanide containing model compounds.

2. Experimental

2.1. Catalysts synthesis and characterization

Two different silica materials were used as supports for the preparation of TiO_2 photocatalysts. The first one was an amorphous SiO_2 commercially available (Grace Sylopol 2104). It presents a wide pore size distribution contrasting with the second silica support, the so-called SBA-15 silica, a mesostructured material with a very well defined pore size in the range of the mesopores (around 6 nm for the material synthesized in this work). The latter was prepared in our laboratory according to the original method of Stucky and co-workers [34].

Incorporation of titania into the supports was carried out through a sol–gel method. Hydrolysis of titanium tetra-isopropoxide and condensation inside the porous structure of the silica was followed by hydrothermal treatment for the crystallization of TiO_2. A detailed explanation of the synthesis procedure can be found elsewhere [32,33]. Depending of the silica support, the catalysts will be named as $x\%TiO_2/GrSiO_2$ or $x\%TiO_2$/SBA-15 (x represents the wt% of titania loading).

In a previous work, the catalysts were characterized by nitrogen adsorption isotherms at 77 K (Micromeritics Tristar 3000) and powder X-ray diffraction (Philips X'PERT MPD, Cu Kα radiation) [32].

In this work, additional characterization has been done in order to clearly establish the structural properties of these materials. Scanning electron microscopy together with energy dispersive X-ray microanalysis was very useful to study the morphology of the particles and the homogeneity in the titania distribution inside the support. SEM micrographs were obtained in a JEOL JSM-6400 working at 20 kV. Transmission electron microscopy (TEM) was used to evaluate the size distribution of the TiO_2 crystals incorporated into the silica. A JEOL JEM-2000 FX microscope working at 200 kV was used to take the TEM micrographs.

Additionally, a more detailed analysis of the porous structure of the TiO_2/SBA-15 photocatalysts has been done, through argon adsorption–desorption isotherms at 77 K, obtained in a Micromeritics ASAP 2010 sorptometer.

2.2. Photocatalytic reactions

The photocatalytic activity of these materials has been tested with different model compounds and their activities have been compared with the results obtained using the commercial TiO_2 sample Degussa P25. The experimental setup consists of a batch photoreactor with irradiation by a 150 W medium pressure mercury lamp (Heraeus TQ-150) externally cooled. The catalyst was maintained in suspension by a magnetic stirrer placed at the bottom of the vessel. A gas bubbling system provides the oxygen required for the oxidation reactions or nitrogen in the cases in which reduction is the main process.

The UV-A incident photon flow, determined by ferrioxalate actinometry, was 1.37×10^{-5} einstein l^{-1} s^{-1}. All reactions were carried out at room temperature with a catalyst concentration of 0.5 g TiO_2 l^{-1}, having in mind the different titania loading of the catalysts tested. This catalyst concentration was previously selected from studies with Degussa P25 titania in order to obtain a total absorption of photons. However, the initial cyanide concentration and initial pH value of the solution depended on the model compound.

Potassium cyanide (Panreac, reagent grade) was used for the free cyanide photoxidation runs. The initial conditions for these reactions were a concentration of 3.85 mM KCN and pH value of 11.0. Cyanide decrease was followed by the pyridine–barbituric standard colorimetric method. Oxidation products, mainly cyanate, were analysed by ion chromatography (Metrohm Separation center 733) using an aqueous solution of $NaHCO_3$ (2.00 mM) and Na_2CO_3 (1.30 mM) as eluent.

Potassium ferricyanide solutions (Panreac, reagent grade) were prepared with an initial concentration of 0.64 mM and pH of 12.0. Total concentration of iron complexed cyanide was determined by ICP/AES (Varian Vista AX), whereas free cyanide and cyanate were analysed by the same methods previously described for potassium cyanide photoxidation runs.

Reactions with potassium dicyanoaurate (Aldrich, 98%) were carried out with an initial concentration of 0.38 mM and pH adjusted to 12.0. Analysis of metal-cyanide complexes was also conducted by ICP/AES and free cyanide and cyanate were determined by the above mentioned methods.

3. Results and discussion

3.1. Characterization of the catalysts

Table 1 summarises the textural properties and average TiO_2 crystal size calculated for these materials, reported in

Table 1
Textural properties and average TiO_2 crystal size of the supported photocatalysts

Catalyst	Specific surface area, S_{BET} ($m^2\ g^{-1}$)	Pore volume, V_P ($cm^3\ g^{-1}$)	Average pore size, D_{BJH} (nm)	Average TiO_2 crystal size, ϕ_{TiO_2} (nm)
Grace SiO_2	317	1.59	19.1	–
20%TiO_2/GrSiO_2	299	1.16	17.1	6.8
40%TiO_2/GrSiO_2	246	0.94	17.5	8.0
60%TiO_2/GrSiO_2	179	0.67	17.3	12.2
SBA-15 SiO_2	640	0.96	6.3	–
20%TiO_2/SBA-15	532	0.78	6.0	6.2
40%TiO_2/SBA-15	442	0.69	5.9	6.7
60%TiO_2/SBA-15	349	0.60	5.8	6.8

the above commented previous work [32], and required for the discussion. The main conclusion of that work was that the use of the SBA-15 silica support seems to control the TiO_2 crystal size by constraining the growing of the titanium dioxide clusters inside the mesoporous channels. In contrast, the use of an amorphous support does not induce this effect, leading to bigger TiO_2 crystals as the titania loading increases.

In the present work, a more detailed characterization of the supported photocatalysts has been done in order to improve the knowledge of the structure of these materials. From the SEM observations, the TiO_2/GrSiO_2 materials consist of 10–70 μm particles. Fig. 1(left) shows the SEM micrograph of a fragment of the 20%TiO_2/GrSiO_2 catalyst. At the bottom of the photograph the silicon and titanium microanalysis performed by X-ray energy dispersive analysis have been included. As it can be seen, this catalyst shows a granular appearance with a heterogeneous distribution of the silicon and titanium oxides. For instance, titanium dioxide seems to be more concentrated in the upper part of this particle. The analysis of several random particles of this material confirmed these results.

In contrast, as it is shown in the SEM micrograph and EDX maps of Fig. 1(right), TiO_2 is apparently more homogeneously distributed in the TiO_2/SBA-15 catalysts. These materials consist of oval shape particles with sizes slightly lower than 1 μm. Maybe this lower size of the silica particles could be responsible of the more homogeneous distribution of the titanium dioxide during the synthesis stage.

In order to find out the crystal size distributions that produce these average values, TEM micrographs were collected. They allow the direct measurement of the size of titanium dioxide particles. However, the small size of the crystals requires such a high enlargement of the image that drastically reduces the number of titania particles observed, making difficult to obtain statistically significant

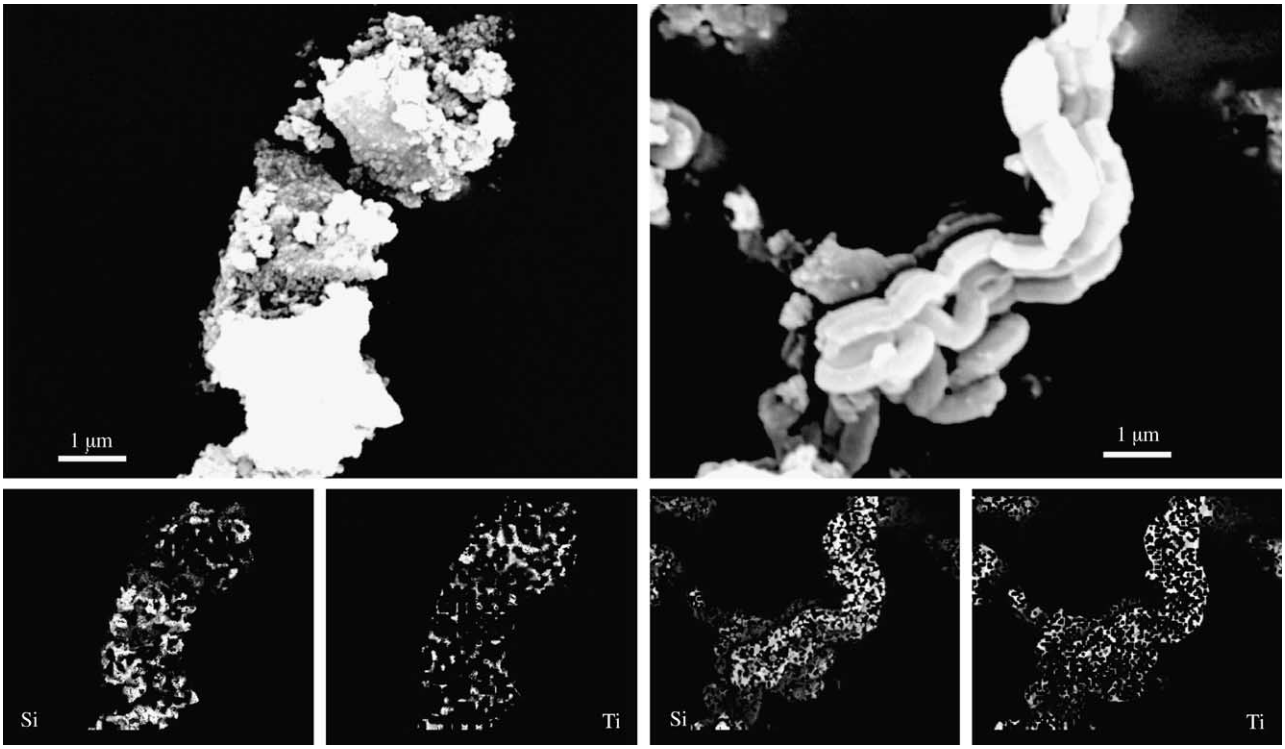

Fig. 1. SEM micrographs and EDX maps of silicon and titanium of the catalysts 20%TiO_2/GrSiO_2 (left) and 20%TiO_2/SBA-15 (right).

results. Consequently, an indirect method was used. A larger area of the catalysts was selected (enough to obtain a substantial amount of TiO_2 crystals) and dark field images were taken. These images are generated by selecting a single direction for electron diffraction. Assuming that the unit cells of the titanium dioxide crystals are randomly orientated, the dark field micrographs produce a statistical high contrast image with very brilliant points whose size depends directly on the crystal size. Fig. 2 displays the TEM micrographs and the corresponding dark field images

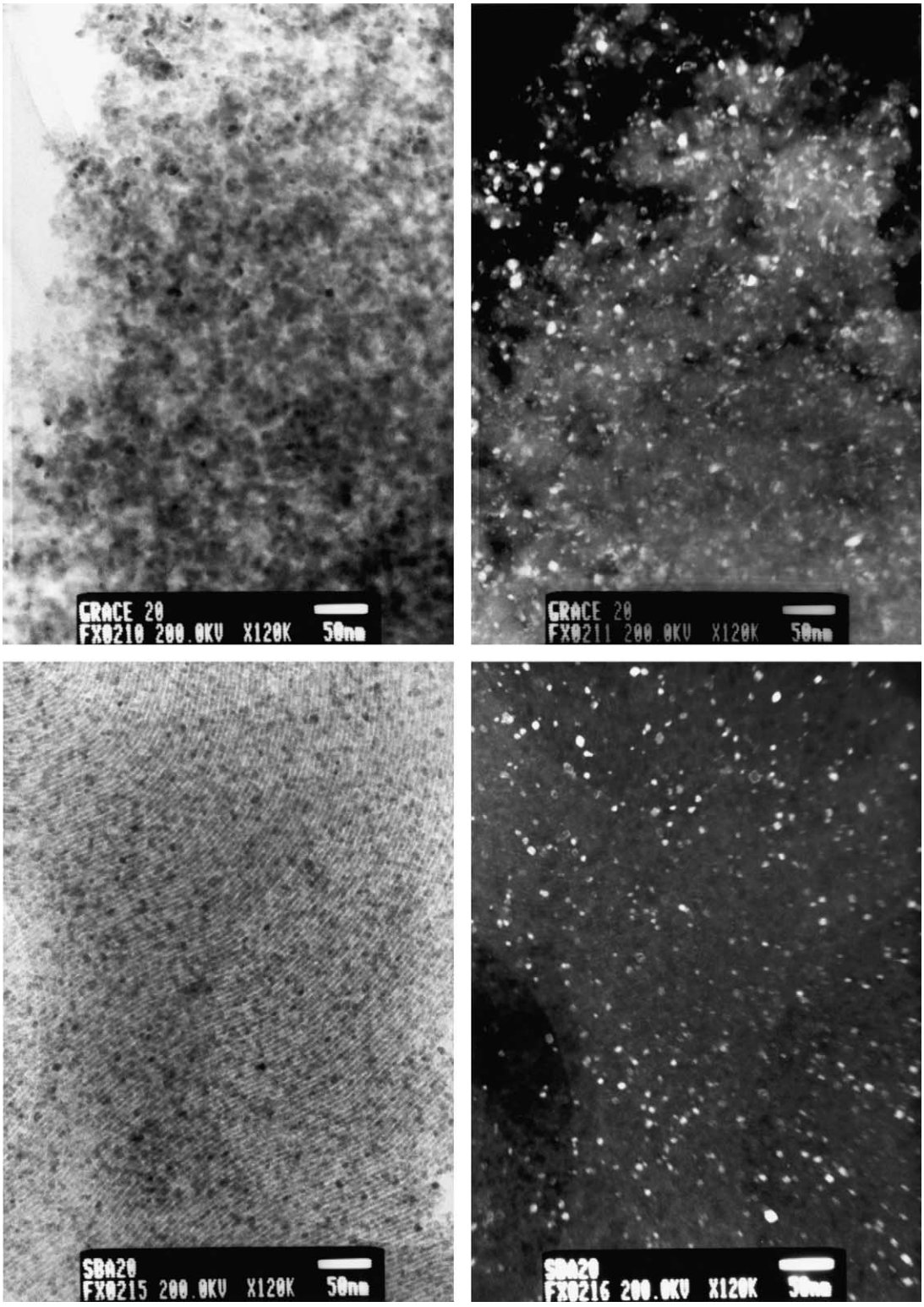

Fig. 2. TEM micrographs (left) and dark field images (right) of the catalysts 20%TiO_2/$GrSiO_2$ (top) and 20%TiO_2/SBA-15 (bottom).

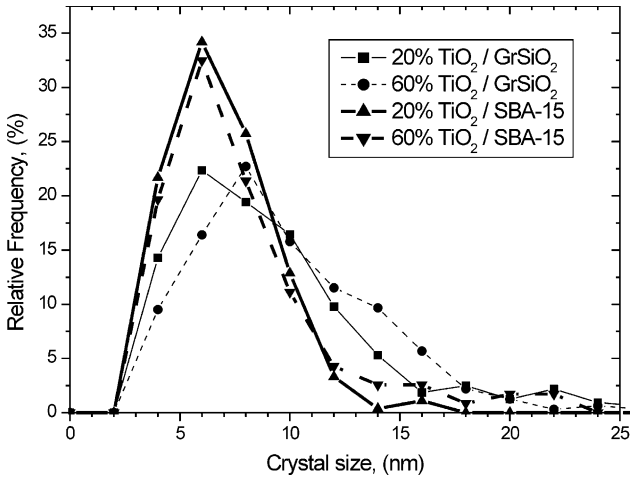

Fig. 3. TiO_2 crystal size distributions of the catalysts supported on amorphous and mesostructured SBA-15 silicas.

of the same area for the catalysts 20%TiO_2/$GrSiO_2$ and 20%TiO_2/SBA-15.

At first sight, titanium dioxide crystals of the 20%TiO_2/SBA-15 material seem to have a more uniform size, whereas the $GrSiO_2$ based catalyst presents a wider range of crystal sizes, although to quantify the distribution, a more accurate procedure must be used. High resolution and contrasted micrographs were processed with the software Olympus MicroImage v4.0 using morphological filters of different shapes in order to count automatically the frequency for every crystal size. Calibration was done by selecting several crystals whose size was clearly measured both in the TEM and in the dark field micrographs. Fig. 3 represents the crystal size distribution obtained for the catalysts with 20 and 60 wt% of TiO_2.

For the catalysts with 20 wt% of TiO_2 the distribution of frequencies obtained with the SBA-15 silica is narrower than that using $GrSiO_2$ as support. For higher titania content, differences induced by both supports are more pronounced. Whereas, the 60%TiO_2/SBA-15 material keeps a titania crystal size distribution very similar to that of 20%TiO_2/SBA-15, the 60%TiO_2/$GrSiO_2$ catalyst shows a shift to bigger TiO_2 crystal sizes in comparison to the catalyst with 20 wt% of TiO_2. These results are in agreement with the average TiO_2 crystal sizes shown in Table 1.

The TEM micrograph of the 20%TiO_2/SBA-15 material shown in Fig. 2 also displays a clear correlation between the regular pore size of the mesostructured SBA-15 support and the crystal size of the titanium dioxide. Additionally, this micrograph also shows that the TiO_2 clusters are located inside the porous of the support with apparently no agglomeration. Consequently, it can be concluded that the SBA-15 pores produce restrictions to the TiO_2 growing, leading to size-controlled silica-supported TiO_2 photocatalysts as it was previously reported [32]. Similar phenomenon has been reported in the literature for the synthesis of particles and nanowires of PbS [35], CdS [36], silicon [37], silver [38,39], gold [39], platinum [39] and palladium [40].

One important question to answer about the TiO_2/SBA-15 catalysts is the possible existence of pore clogging of the mesoporous channels by the titanium dioxide crystals. The presence of these particles inside the pores of the SBA-15 would suggest the existence of accesibility problems to the active phase, especially for high titania loadings. However, the results of pore volume reported in Table 1 discard this phenomenon, at least for the low molecular size of the molecular nitrogen used for the adsorption–desorption isotherms. In fact, the pore volumes of the supported photocatalysts are consistent with their silica content. In a previous work [32], we suggested that the micropore network that some authors have identified interconnecting the mesoporous channels [41,42] could be responsible of the total absence of pore clogging effects. The formation of this micropores is produced during the synthesis stage of the SBA-15 silica and is due to the penetration of the polyethyleneoxide chain in the silica walls, leading to micropores when calcinating. A recent work [43] has demonstrated the correlation between the micropore structure of these materials and the treatment followed for surfactant removal. Argon adsorption isotherms in the range of very low pressures were collected, in order to obtain information about the microporous structure of the TiO_2/SBA-15 materials. The micropores size distributions have been calculated by applying the *Hovart–Kawazoe* method. For the SBA-15 silica a very narrow distribution with a maximum in 1.05 nm is obtained, whereas for the 20%TiO_2/SBA-15 photocatalyst, a wider plot is found with a maximum in 1.30 nm. This broadening is probably due to both the hydrothermal treatment followed for the titanium dioxide crystallization and some microporosity generated by the titania particles located in the mesoporous channels.

Additionally, the micropore and mesopore volumes of these materials can be estimated by using the *t*-plot graphs calculated from the adsorption branch of the nitrogen adsorption–desorption isotherms. The *t*-plot graphs of the SBA-15 related materials could be divided in two zones: Zone I (at low partial pressures) is related to the micropores, and the extrapolation of the lineal part of the graph leads to the micropore volume of the material; Zone II (at intermediate-high partial pressures) is related to the mesopores, leading by extrapolation to the sum of micropores and mesopores volumes. The results obtained for the SBA-15 silica are 0.145 $cm^3\ g^{-1}$ of micropores and 0.681 $cm^3\ g^{-1}$ of mesopores. These values represent the 15.0 and 70.8%, respectively, of the total pore volume shown in Table 1.

Concerning the 20%TiO_2/SBA-15 photocatalyst, 0.114 $cm^3\ g^{-1}$ of micropores and 0.493 $cm^3\ g^{-1}$ of mesopores are obtained, representing the 14.8 and 63.9%, respectively, of the total pore volume of this material. Taking into account that the nanocrystals of titanium dioxide incorporated to the silica can be considered as non-porous, all volumes calculated for the supported catalysts are consistent with the 80% of

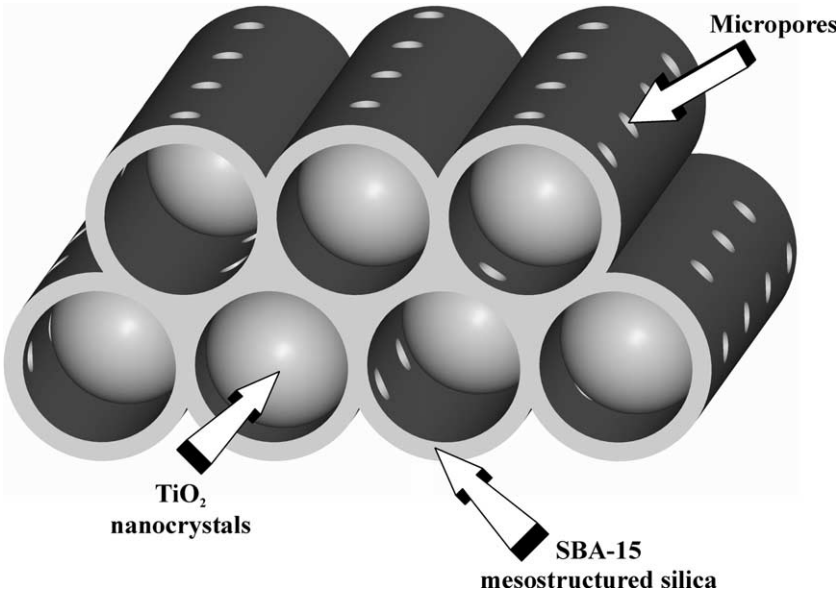

Fig. 4. Schematic representation of the structure proposed for the TiO_2/SBA-15 photocatalysts.

silica content. Micropore volume fraction is very similar to the support, whereas the lower contribution of mesopores to the total pore volume is consistent with the presence of the titanium dioxide particles inside these channels.

Results for 20%TiO_2/SBA-15 definitively establish the existence of a microporous network similar to that of the SBA-15 structure. Consequently, we propose for the TiO_2/SBA-15 photocatalysts the structure schematized in Fig. 4. It can be considered that these materials are constituted by TiO_2 crystals located inside the channels of the support, whose walls constrain their growing in the synthesis stage. According to this structure, diffusion could be mainly restricted to the micropore network interconnecting the mesopores.

In contrast, the results displayed in Table 1 for the TiO_2/$GrSiO_2$ materials clearly show a more drastic reduction in the pore volume of these materials when increasing titania loading. Those values are even lower than that corresponding to their silica content, that means that in this case the porous structure of the support is partially clogged when incorporating titanium dioxide, since no micropores are connecting the mesoporous network.

3.2. Photocatalytic activity

Initially, photoxidation of free cyanide to cyanate was carried out with the supported photocatalysts. A reaction using Degussa P25 was also performed in the same experimental conditions with the aim of comparison. Taking into account that photocatalysis is a process involving the catalyst surface, it would be desirable to compare the performance of the studied catalysts considering their respective surface areas. The estimation of the latter values is, however, difficult to do in supported titania. The use of the total surface area of the catalysts is not acceptable, as the TEM micrographs show that titania is not supported on silica as a layer but as particles. Another approach could be a calculation of the TiO_2 surface in the materials assuming non-porous spherical semiconductor nanoparticles. This gives values in a range of 3–5 times the surface of the equivalent weight of Degussa P25. However, the truly accessible titania surface must be necessary lower because the semiconductor nanoparticles are supported on the silica. Considering this inaccuracy for measuring the real TiO_2 surface area, instead of the surface related reaction rate expression, we have used the volume related reaction rate values for the comparison of the catalysts. It should be also noticed that from a technical point of view such parameter can be quite convenient in order to compare the performance of the different catalysts with the same titania weight.

Table 2 reports the initial reaction rate values (r^0) of the studied catalysts for free cyanide photoxidation. These values have been normalised to the activity of Degussa P25 in order to facilitate the comparison of the results obtained throughout the different reactions tested in this work.

As it can be seen from Table 2, for equal mass titania content all the supported catalysts show lower activities than the P25 TiO_2 in this reaction. However, important differences are obtained depending on the titania loading and the kind of silica support. With both supports an increase

Table 2
Activity of the catalysts for free cyanide photoxidation

Photocatalyst	r^0 ($mg_{CN}\, l^{-1}\, min^{-1}$)	r^0/r^0_{P25}
Degussa P25	1.5400	1.0000
20%TiO_2/$GrSiO_2$	0.7514	0.4879
40%TiO_2/$GrSiO_2$	0.8533	0.5541
60%TiO_2/$GrSiO_2$	0.9838	0.6389
20%TiO_2/SBA-15	1.0300	0.6688
40%TiO_2/SBA-15	1.1144	0.7236
60%TiO_2/SBA-15	1.3054	0.8477

in the reaction rate is observed as the titanium dioxide wt% increases, but SBA-15 based photocatalysts show higher activities than $GrSiO_2$ based materials with the same TiO_2 loading.

These results suggest that the intrinsic activity of the size-controlled titania crystals in the TiO_2/SBA-15 materials is much higher than that obtained with the use of an amorphous support. This high activity, however, is always lower than the reaction rate achieved with the P25 catalyst, reaching at most an 85% of the latter value with the 60%TiO_2/SBA-15 material. This fact confirms that for free cyanide photoxidation a decrease in activity must be probably assumed when supporting TiO_2.

To study if the structural properties of the silica-supported materials have analogous influence in the photocatalytic degradation of other cyanide containing compounds, reactions with hexacyanoferrate-(III) and dicyanoaurate complexes were carried out.

Hexacyanoferrate-(III) is a metal-cyanide complex that release free cyanide ions to the medium on exposure of its aqueous solutions to UV light. The photodegradation of this compound takes place through a previous photolytic breakage of the complex followed by the photocatalytic oxidation of the released CN^- ions to cyanate species. More details about the degradation mechanism of iron cyanocomplexes can be found elsewhere [44].

As it can be seen in Table 3, despite the high activity exhibited by P25 TiO_2 for free cyanide solutions photoxidation, comparing to the TiO_2/SiO_2 catalysts a very low oxidation activity is obtained when CN^- species come from iron-cyanide complexes present in the medium. In contrast, the supported photocatalysts lead to better results in the cyanide photoxidation rate, up to eight times higher for the 20%TiO_2/SBA-15 catalyst. Also the effect of the titania loading is different in this second reaction according to the activity shown by SBA-15 catalysts containing 40 and 60 wt% of TiO_2. In this case, a lower oxidation activity is obtained as the titanium dioxide content increases.

To explain this fact, we must refer to both the mechanism of the reaction and the structure of the TiO_2/SBA-15 materials. Considering that the released cyanide ions and not the whole iron complex are those that have to get the titania surface to be oxidised, a higher activity is expected if the access of the iron cyanocomplex to the titania particles becomes restricted in favour of the cyanide ions [44]. As it has been seen in the first part of the work, the TiO_2/SBA-15 materials consist of TiO_2 clusters located inside the porous of the silica structure. The micropore network interconnecting the mesoporous SBA-15 channels can be proposed as responsible of the absence of pore clogging in this catalyst, but obviously referred only to molecules of small sizes such as CN^-. If we consider, however, the molecular size of the hexacyanoferrate-(III) complex such micropores can act as a molecular sieve hindering its access through the whole porous network and then to the TiO_2 surface. Consequently, it is expected that this selectivity for CN^- promoted by the SBA-15 support is enhanced for low titania loading, as the reactants have to cover longer average distances inside the porous structure of the silica support to get the titania surface. This would explain not only the results obtained with the TiO_2/SBA-15 catalysts but also with Degussa P25 TiO_2, in which the access of the iron cyanocomplexes to the TiO_2 clusters is not restricted.

In order to obtain further experimental verifications for this hypothesis, experiments of photocatalytic treatment of dicyanoaurate complex solutions were carried out. The main difference of this metal-cyanide complex respect to hexacyanoferrate-(III) is that the former is stable under UV irradiation, not producing photolytic release of CN^-. Therefore, in this case, the complex must reach the TiO_2 surface where the gold atoms are reduced to Au(0), then releasing free cyanide ions.

Assuming the molecular sieve behaviour of the 20%TiO_2/SBA-15 structure, in this case its activity would be much lower than that obtained with the catalyst 60%$TiO_2/GrSiO_2$. The experimental results shown in Table 4 confirm this hypothesis. As it can be seen, the reaction rate value achieved with the 20%TiO_2/SBA-15 catalyst is fivefold lower than that corresponding to the 60%$TiO_2/GrSiO_2$. Moreover, in this case the activity of the latter is even higher than the value for Degussa P25. This effect could be due to the adsorption properties of the silica and its nature is now under further investigations.

Summarising, the activities of the different photocatalysts for the tested reactions show the following decreasing order:

(i) Free cyanide photoxidation: Degussa P25 > TiO_2/SBA-15 > $TiO_2/GrSiO_2$.
(ii) Cyanate production in hexacyanoferrate photodegradation: TiO_2/SBA-15 > $TiO_2/GrSiO_2$ > Degussa P25.
(iii) Dicyanoaurate photoreduction: $TiO_2/GrSiO_2$ > Degussa P25 > TiO_2/SBA-15.

Table 3
Activity of the catalysts for hexacyanoferrate-(III) photodegradation

Photocatalyst	r^0 ($mg_{OCN}\,l^{-1}\,min^{-1}$)	r^0/r^0_{P25}
Degussa P25	0.0330	1.000
20%$TiO_2/GrSiO_2$	0.0501	1.520
20%TiO_2/SBA-15	0.2622	7.956
40%TiO_2/SBA-15	0.1619	4.912
60%TiO_2/SBA-15	0.0997	3.025

Table 4
Activity of the catalysts for dicyanoaurate photodegradation

Photocatalyst	r^0 ($mg_{Au}\,l^{-1}\,min^{-1}$)	r^0/r^0_{P25}
Degussa P25	0.3392	1.000
60%$TiO_2/GrSiO_2$	0.4563	1.345
20%TiO_2/SBA-15	0.0982	0.289

We propose that the results obtained can be explained in terms of the molecular sieve behaviour shown by SBA-15 support. The micropore network that interconnects the channels of the SBA-15 mesoporous structure acts by limiting the size of the molecules that can reach the titania surface to be photocatalytically degradated.

4. Conclusions

The results presented in this work point out the strong influence of the textural properties of the silica on the catalytic activities of the supported TiO_2 photocatalysts. The elucidation of the structure of the TiO_2/SBA-15 photocatalysts has permitted to explain the differences observed in the reaction rate values shown by these materials in comparison with the use of an amorphous silica support.

As a general conclusion, it must be pointed out that to achieve an absolute assessment of the activity of new developed photocatalysts, several model compounds should be tested. This is especially important in the case of supported catalysts where the structure of the support can be crucial.

Acknowledgements

The authors thank ‘‘Consejería de Educación, Comunidad de Madrid’’ for the financial support of this research through the project ‘‘Contrato-Programa Grupos Estratégicos de Investigación’’ and ‘‘Ministerio de Ciencia y Tecnología’’ through the project PPQ2000-1287.

References

[1] D.F. Ollis, E. Pellizzetti, N. Serpone, Environ. Sci. Technol. 25 (1991) 1522.
[2] M.A. Fox, M. Dulay, Chem. Rev. 93 (1993) 341.
[3] O. Legrini, E. Oliveros, A.M. Braun, Chem. Rev. 93 (1993) 671.
[4] D.F. Ollis, H. Al-Ekabi (Eds.), Photocatalytic Purification and Treatment of Water and Air, Elsevier, Amsterdam, 1993.
[5] M.R. Hoffmann, S.T. Martin, W. Choi, D.W. Bahnemann, Chem. Rev. 95 (1995) 69.
[6] J.M. Herrmann, Catal. Today 53 (1999) 115.
[7] D. Blake, Bibliography of work on the photocatalytic removal of hazardous compounds from water and air, NREL/TP-510-31319, Golden, National Renewable Energy Laboratory, CO, USA, 2001.
[8] R.L. Pozzo, M.A. Baltanás, A.E. Cassano, Catal. Today 39 (1997) 219.
[9] J.A. Byrne, B.R. Eggins, N.M.D. Brown, B. McKinney, M. Rouse, Appl. Catal. B: Environ. 17 (1998) 25.
[10] J.M. Herrmann, J.L. Mansot, J. Catal. 121 (1990) 340.
[11] V. Augugliaro, V. Loddo, G. Marcí, L. Palmisano, M.J. López-Muñoz, J. Catal. 166 (1997) 272.
[12] H. Yamashita, Y. Ichihashi, M. Harada, G. Stewart, M.A. Fox, M. Anpo, J. Catal. 158 (1996) 97.
[13] J.M. Herrmann, H. Tahiri, C. Guillard, P. Pichat, Catal. Today 54 (1999) 131.
[14] V. Romeas, P. Pichat, C. Guillard, T. Chopin, C. Lehaut, Ind. Eng. Chem. Res. 38 (1999) 3878.
[15] H. Yamashita, M. Honda, M. Harada, Y. Ichihashi, M. Anpo, T. Hirao, N. Itoh, N. Iwamoto, J. Phys. Chem. B 102 (1998) 10707.
[16] G. Lassaleta, A. Fernández, J.P. Espinos, A.R. González-Elipe, J. Phys. Chem. 99 (1995) 1848.
[17] H. Inoue, T. Matsuyama, B.J. Liu, T. Sakata, H. Mori, H. Yoneyama, Chem. Lett. (1994) 653.
[18] A. Yasumori, K. Yamazaki, S. Shibata, M. Yamane, J. Ceram. Soc. 102 (1994) 702.
[19] R. Castillo, B. Koch, P. Ruiz, B. Delmon, J. Catal. 161 (1996) 524.
[20] M.L. Franco-García, M. Murat, J.P. Percherancier, B. Pouyet, Fresenius Environ. Bull. 5 (1996) 563.
[21] G.P. Lepore, L. Persaud, C.H. Langford, J. Photochem. Photobiol. A: Chem. 98 (1996) 103.
[22] Q. Dai, N. He, K. Weng, B. Lin, Z. Lu, C. Yuan, J. Inclusion Phenom. Macroc. Chem. 35 (1999) 11.
[23] K. Kobayakawa, C. Sato, Y. Sato, A. Fujishima, J. Photochem. Photobiol. A: Chem. 118 (1998) 65.
[24] Z. Ding, X. Hu, G.Q. Lu, P.L. Yue, P.F. Greenfield, Langmuir 16 (2000) 6216.
[25] Z. Ding, X. Hu, P.L. Yue, G.Q. Lu, P.F. Greenfield, Catal. Today 68 (2001) 173.
[26] R.J. Davis, Chem. Mater. 4 (1992) 1410.
[27] Y. Xu, C.H. Langford, J. Phys. Chem. B 101 (1997) 3115.
[28] H. Yamashita, Y. Fujii, Y. Ichihashi, S.G. Zhang, K. Ikeue, D.R. Park, K. Koyano, T. Tatsumi, M. Anpo, Catal. Today 45 (1998) 221.
[29] B.J. Aronson, C.F. Blanford, A. Stein, Chem. Mater. 9 (1997) 2842.
[30] N. Takeda, T. Torimoto, S. Sampath, S. Kuwabata, H. Yoneyama, J. Phys. Chem. 99 (1995) 9986.
[31] H. Yoneyama, T. Torimoto, Catal. Today 58 (2000) 133.
[32] R. van Grieken, J. Aguado, M.J. López-Muñoz, J. Marugán, J. Photochem. Photobiol. A 148 (2002) 315.
[33] J. Aguado, R. van Grieken, M.J. López-Muñoz, J. Marugán, Catal. Today 75 (2002) 95.
[34] D. Zhao, J. Feng, Q. Huo, N. Melosh, G.H. Fredickson, B.F. Chmelka, G.D. Stucky, Science 279 (1998) 548.
[35] F. Gao, Q. Lu, X. Liu, Y. Yan, D. Zhao, Nano Lett. 1 (2001) 743.
[36] W. Xu, Y. Liao, D.L. Akins, J. Phys. Chem. B 106 (2002) 11127.
[37] N.R.B. Coleman, N. O'Sullivan, K.M. Ryan, T.A. Crowley, M.A. Morris, T.R. Spalding, D.C. Steytler, J.D. Holmes, J. Am. Chem. Soc. 123 (2001) 7010.
[38] M.H. Huang, A. Choudrey, P. Yang, Chem. Commun. (2000) 1063.
[39] Y.J. Han, J.M. Kim, G.D. Stucky, Chem. Mater. 12 (2000) 2068.
[40] I. Yuranov, P. Moeckli, E. Suvorova, P. Buffat, L. Kiwi-Minsker, A. Renken, J. Mol. Catal. A: Chem. 192 (2003) 239.
[41] M. Kruk, M. Jaroniec, Chem. Mater. 12 (2000) 1961.
[42] A. Galarneau, H. Cambon, F. Di Renzo, R. Ryoo, M. Choi, F. Fajula, New. J. Chem. 27 (2003) 73.
[43] R. van Grieken, G. Calleja, G.D. Stucky, J.A. Melero, R.A. García, J. Iglesias, Langmuir 19 (2003) 3966.
[44] R. van Grieken, J. Aguado, M.J. López-Muñoz, J. Marugán, Appl. Catal. B: Environ. 55 (2004) 195.